Effect of MgO additive on catalytic properties of Co/SiO2 in the dry reforming of methane

Rabah Bouarab, O. Akdim, Aline Auroux, Ouiza Chérifi, Claude Mirodatos

Effect of MgO additive on catalytic properties of Co/SiO_2 in the dry reforming of methane

R. Bouarab [a,b], O. Akdim [b], A. Auroux [b], O. Cherifi [a], C. Mirodatos [b,*]

[a] *Laboratoire de Chimie de Gaz Naturel, Faculté de Chimie, U.S.T.H.B., P.O. Box 32, 16111 El Alia, Bab Ezzouar, Algeria*
[b] *Institut de Recherches sur la Catalyse, CNRS, 2 Avenue Albert Einstein, 69626 Villeurbanne Cedex, France*

The dry reforming of methane to syngas was studied in the temperature range 500–800 °C on a series of Co/SiO_2 catalysts modified by MgO (5–35 wt.%). The materials have been prepared by successive incipient wetness impregnation and characterised by BET, XRD, H_2-TPR, CO_2 adsorption and in situ-DRIFT. The formation of a silicate adlayer Mg_2SiO_4 is observed at high MgO content (30–35 wt.%), which corresponds to a much improved catalytic stability under the severe dry reforming conditions. This phase favours the development of small metallic cobalt particles, preventing their coalescence under reaction conditions. A bi-functional mechanism is proposed which combines the accumulation of oxidizing agents like carbonates and hydrogeno-carbonate adspecies on the catalyst support due to a medium basicity of the layer and the reactivity of small metal particles for methane activation. This concerted process tends to limit coke formation and therefore contribute to the observed catalytic stability.

Keywords: Methane dry reforming to syngas; Co/SiO_2 catalyst; MgO additive; Silicate layer

1. Introduction

The conversion of methane by carbon dioxide, is called 'dry reforming':

$$CH_4 + CO_2 \rightarrow 2CO + 2H_2 \quad \Delta H^{\circ}_{298} = +247\,\mathrm{kJ\,mol^{-1}} \quad (1)$$

It remains of strategic interest, essentially since it provides a CO/H_2 ratio adapted to the gas-to-liquid process (methanol and Fischer-Tropsch synthesis of sulfur free higher hydrocarbons) [1]. In addition, this endothermic reaction can be used together with the reverse exothermic carbon monoxide hydrogenation, for storage and transport of solar or nuclear energy to consumption centres, following the thermochemical heat pipe concept [2]. In spite of a large range of catalysts currently used for this reaction, deactivation by coke deposition remains the main drawback of the reaction [1–7]. Metal and metal oxide modifiers, in particular basic additives [1,7,8], have been shown to strongly modify the rate of coke deposition on the active phase [9]. Thus, it has been shown that the addition of MgO increases the activity of Rh/SiO_2 catalysts by activating dissociation of carbon dioxide [10]. Resistance to coking has also been obtained by adding CeO_2 [6] or La_2O_3 [11] to nickel-based catalyst.

As an alternative to nickel-based catalysts which always present the drawback of possible methanation in the downstream gas tail with the extracted catalyst fines, cobalt-based catalysts were also shown to be active for dry reforming reaction [12–17]. For these catalysts the interaction between metal and support was also found to strongly influence reducibility [14,18,19] and therefore catalytic activity. As observed for noble metals, addition of magnesia was found to stabilise somehow the catalytic activity for a lab-scale ageing period [7] and the presence of CoO–MgO solid solution in Co(O)/MgO was tentatively proposed to be responsible for this effect [17]. It has also been assumed that magnesia could inhibit coke deposition via adsorbed CO_2 species on the catalyst surface, able to react with the deposited carbon through the reverse Boudouard reaction [7]. Preliminary results confirming this positive effect of MgO (or La_2O_3) addition were presented in [20] on a

* Corresponding author. Tel.: +33-472-44-5366; fax: +33-472-44-5399.
E-mail address: mirodatos@catalyse.cnrs.fr (C. Mirodatos).

reference Co/SiO_2 catalyst. A direct relationship was observed between the acid–base properties of the catalysts, as determined by isopropanol conversion, and coke deposition. In this study, we present new results on the effect of MgO additive on catalytic activity, stability and coking properties of Co/SiO_2 in the reaction of dry reforming of methane, by considering the effect of magnesia additive concentration on the solid state changes in the catalyst structure.

2. Experimental

2.1. Catalyst preparation

Supported 5 wt.% cobalt catalysts were prepared by successive incipient wetness impregnation as follows: the supports x wt.% MgO–SiO_2 ($x = 0$, 5, 10 or 35) were prepared by impregnating silica (Aerosil from Degussa, $BET_{area} = 196\,m^2/g$) with appropriate solutions of magnesium nitrate $Mg(NO_3)_2{\cdot}6H_2O$. After drying at 110 °C overnight and calcining under oxygen at 500 °C for 4 h, a second incipient wetness impregnation was carried out by using hexahydrated cobalt nitrate ($Co(NO_3)_2{\cdot}6H_2O$, Rhone-Poulenc). The resulting solids were dried and calcined once more under the same conditions. The catalysts obtained are $Co(O)/SiO_2$, Co(O)/5 wt.% MgO–SiO_2, Co(O)/10 wt.% MgO–SiO_2 and Co(O)/35 wt.% MgO–SiO_2 (Co(O) = cobalt oxide). Composition and BET area are reported in Table 1.

2.2. Catalysts characterisation and testing

Inductive coupled plasma emission spectroscopy (Spectro-Analytical Instruments ICP-D) was used to determine cobalt and magnesium oxide contents in the catalysts after dissolving the samples in a mixture of hydrofluoric, nitric and sulphuric acids. Carbon deposits were analysed by coulometric detection of CO_2 emission.

After pretreatment at 200 °C under vacuum, multipoint BET surface area measurements were performed using nitrogen as an adsorbate at −196 °C.

A Philips PW 1050/81 diffractometer was used to obtain X-ray diffraction patterns over a range of 5–80 2θ degrees. The acquisition period was 1.0 s/step. Cu Kα: 45 kV, 35 mA, $\lambda = 1.54$ Å was used as the X-ray source. The catalysts were examined both before and after the reaction.

Temperature programmed reduction (TPR) profiles were determined by a continuous flow technique. The catalyst samples, 200 mg, were flushed with argon in a quartz reactor tube with 4 mm i.d., heated at 150 °C for 1 h and cooled down to 20 °C, after which H_2-TPR was performed. The reduction gas 1% H_2/Ar and argon reference gas were admitted onto the samples with a fixed mass flow of 19 ml/min. The samples were then heated from 20 to 800 °C using a temperature gradient of 5 °C/min. The effluent gas was passed through a molecular sieve trap to remove water.

Measurements of samples basicity were performed by carbon dioxide adsorption at 80 °C in a micro-calorimeter. Prior to any adsorption the samples were pretreated under hydrogen at 600 °C overnight before being evacuated 2 h at the same temperature and then placed in the calorimeter. Differential heats of adsorption of carbon were measured in a heat flow micro-calorimeter (Setaram HT) linked to a volumetric adsorption system. Successive small doses of CO_2 were sent over the catalyst. Adsorbed amount and heat released were determined simultaneously at every coverage. From the calorimetric and volumetric data, the differential heats of adsorption versus coverage and the corresponding isotherms are plotted.

In situ DRIFT measurements were carried out by using a Spectratech heating cell adapted to a NICOLET 550 FTIR spectrometer. Samples were first reduced in situ under

Table 1
Physico-chemical and catalytic properties of the MgO modified Co/SiO_2 catalysts

Catalyst	Composition (wt.%)		BET area (m^2/g)	CO_2 adsorption[a] ($\mu mol/m^2$)	Catalytic properties at 600 °C			
	Co	MgO			Reaction conditions[b]	CH_4 conversion (%)	CO_2 conversion (%)	Coke formation[c] (wt.%)
Co/SiO_2	4.7	0	185	∼0	Initial	41.0	64.5	
					After 3 h	16.2	29.7	0.41
Co/5 wt.% MgO–SiO_2	4.7	4.4	178	0.013	Initial	42.3	65.3	
					After 3 h	10.5	2.9	0.29
Co/10 wt.% MgO–SiO_2	4.9	9.1	214	0.037	Initial	40.2	61.1	
					After 3 h	9.7	2.0	0.32
Co/35 wt.% MgO–SiO_2	3.9	32.4	191	0.164	Initial	42.1	70.0	
					After 3 h	42.4	69.7	ε[d]
					Thermodynamic equilibrium	42.7	55.6	

[a] Amount of adsorbed CO_2 under an equilibrium pressure of 0.5 Torr as measured in a micro-calorimeter.
[b] Temperature = 600 °C, total pressure = 1 atm, flow rate = 22 ml/min (Co/MgO and MgO–SiO_2 samples showed no reactivity).
[c] Measured after 12 h reaction.
[d] Traces, below 0.1 wt.%.

flowing hydrogen (10 ml/min at 600 °C for 1 h). Then the catalysts were contacted either with diluted CO_2 (10% in He) or with diluted CH_4 (10% in He) or with reacting mixture CH_4/CO_2/He (10/10/80 vol.%). Spectra were recorded with a resolution of 4 cm^{-1} and the background recorded under similar conditions with KBr was subtracted to each corresponding spectra.

Catalysts were tested under atmospheric pressure in a fixed-bed quartz tubular reactor after reduction in situ for 2 h at 600 °C under pure hydrogen with a heating rate of 4 °C/min, and using an amount of catalyst of 100 mg for all runs, particle size $\leq$0.2 mm. After reduction from room temperature to 600 °C, the reacting gases (CH_4/CO_2/He = 10/10/80 vol.%) were introduced into the reactor at a total flow rate of 22 ml/min. Two procedures were applied: (i) the reaction was carried out at the same temperature, 600 °C, for isothermal steady-state ageing tests (as a function of time on stream); (ii) the temperature was first decreased to 500 °C then the reacting gases were admitted, and the reaction temperature was increased step by step till 800 °C, then decreased down to 500 °C for checking the catalysts' stability under temperature cycling conditions. The reacting gases and products were analysed by a TCD chromatograph (HP 6890 GC system) using a Porapak Q column and by mass spectrometry (GASLAB 300). Temperature of the catalyst bed was monitored using a chromel-alumel thermocouple.

3. Results and discussion

3.1. XRD measurement

The general aspect of XRD spectra of freshly calcined catalysts is shown in Fig. 1. With the undoped Co(O)/SiO_2 sample (spectrum (1)), a well-crystallised Co_3O_4 cubic crystalline phase can be observed at angles 2θ = 31.3, 36.8, 44.9, 59.4 and 65.5° [21]. Addition of 5–10 wt.% MgO, curves (2) and (3), respectively, decreases the intensity of crystalline Co_3O_4 peaks. This indicates that part of the cobalt oxide phase is in strong interaction with MgO. As a matter of fact, both cobalt and magnesium oxide have an NaCl-type structure with almost the same lattice parameters and bond distances [17]. So, CoO and MgO are miscible and can form a solid solution [17,21]. At higher MgO loading (35 wt.%, curve (4)) the 2θ = 23° band, characteristic of SiO_2, is markedly decreased and shifted towards higher 2θ values (around 25°), while new bands are formed at 2θ = 35.7, 36.5, 52.2, 62.0 and 69.6° as pointed out in Fig. 1 by cross symbols. These new bands are characteristic of forsterite-type Mg_2SiO_4 silicate, where the cations Mg^{2+} are packed with $(SiO_4)^{2-}$ tetrahedra [22,23]. They demonstrate the occurrence of the solid–solid reaction between silica and magnesium oxide during heat treatments. Though partly overlapping with the bands of the Mg_2SiO_4 silicate (for the diffraction angles 2θ = 36.853 and 36.547, respectively), the bands characteristic of well-crystallised Co_3O_4 (dot symbols in Fig. 1) are slightly reinforced as compared to spectrum 3 (10 wt.% MgO–SiO_2) but also enlarged, indicating a better dispersion. This reappearance of the Co_3O_4 bands at high Mg loading will be ascertained after high temperature cyclic treatments as pointed out later (Fig. 6, spectrum 4). Thus, after mixing cobalt oxide and 35 wt.% MgO–SiO_2, it can be seen that (i) a new Mg_2SiO_4 phase is formed and (ii) the Co_3O_4 phase which was progressively reacting with MgO to form a MgCoO solid solution for lower MgO content [17], is now preserved from reacting with magnesia and more dispersed (stronger and larger bands). In other words, the formation of the Mg_2SiO_4

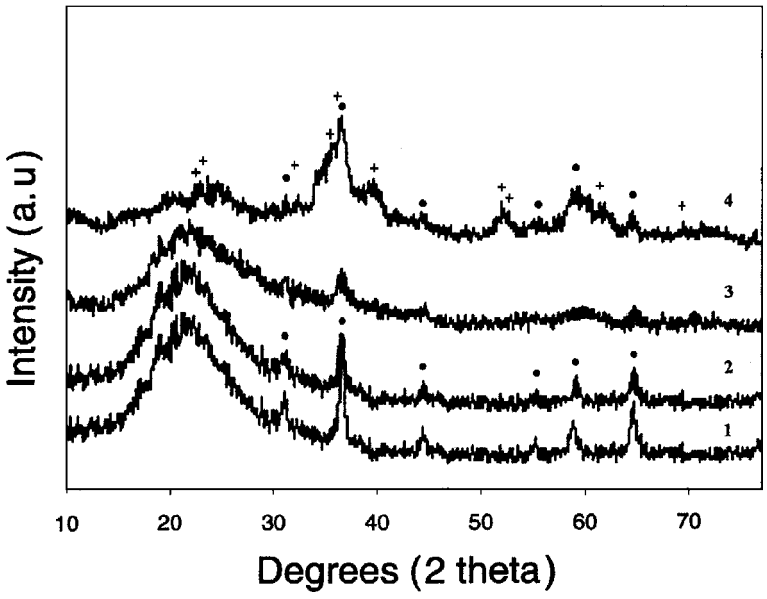

Fig. 1. XRD patterns of (1) Co(O)/SiO_2, (2) Co(O)/5 wt.% MgO–SiO_2, (3) Co(O)/10 wt.% MgO–SiO_2 and (4) Co(O)/35 wt.% MgO–SiO_2: (●) Co_3O_4, (+) Mg_2SiO_4.

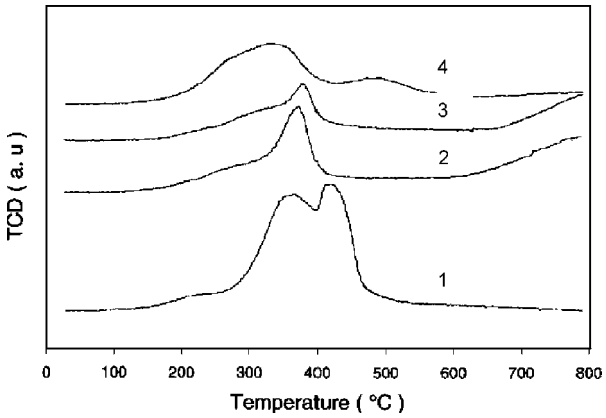

Fig. 2. TPR profiles of (1) Co(O)/SiO_2, (2) Co(O)/5 wt.% MgO–SiO_2, (3) Co(O)/10 wt.% MgO–SiO_2 and (4) Co(O)/35 wt.% MgO–SiO_2.

silicate phase at high MgO content tends to restrict the formation of a solid solution between cobalt oxide and MgO, therefore ensuring a better dispersion of the 5 wt.% Co_3O_4 phase.

3.2. H_2-TPR of catalysts

The H_2-TPR spectra obtained for Co(O)/SiO_2, Co(O)/5 wt.% MgO–SiO_2, Co(O)/10 wt.% MgO–SiO_2 and Co(O)/35 wt.% MgO–SiO_2 catalysts are plotted in Fig. 2. For Co(O)/SiO_2 (curve 1), the cobalt oxide was reduced between 280 and 500 °C with two well separated peaks with maxima at 370 and 425 °C. This two-step reduction pattern, as generally agreed in the literature [12,13,24], corresponds to the primary reduction of Co_3O_4 to CoO (first maximum at 370 °C), followed by the reduction of CoO to metallic cobalt around 425 °C. After 5–10 wt.% MgO addition (curves 2 and 3), the two above described peaks tend to merge into a single one around 380–400 °C (the intensity of which is decreasing with MgO content) while a much larger new peak high temperature starts at around 650 °C and still increases at 800 °C. In agreement with XRD results, the merged peak at 380–400 °C can be assigned to the easier and almost direct reduction of the remaining Co_3O_4 to metallic cobalt phase, while the high temperature hydrogen consumption would correspond to the difficult reduction of the solid solution Co–Mg–O. After 35 wt.% MgO addition (curve 4), mainly two broad reduction peaks at 335 and 480 °C are observed, practically without hydrogen consumption at high temperature. Again on the basis of the XRD results, it can be proposed that the first large peak corresponds, like for the unpromoted Co(O)/SiO_2 sample, to the easy reduction of Co_3O_4 to well dispersed CoO (due to the existence of the silicate layer), while the smaller second peak corresponds to the formation of small cobalt metal particles. From the qualitative integrated band intensity, it may also be deduced that part of the cobalt (few %) remains unreduced for this case, probably due to silicate decoration.

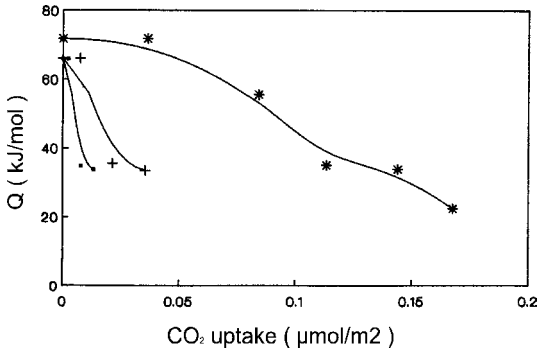

Fig. 3. Differential heats of CO_2 adsorption of (■) Co(O)/5 wt.% MgO–SiO_2, (+) Co(O)/10 wt.%MgO–SiO_2 and (*) Co(O)/35 wt.% MgO–SiO_2.

3.3. Basicity measurements by micro-calorimetry

Changes in surface basicity as a function of MgO content were investigated by CO_2 adsorption carried out at 80 °C. The differential heats of CO_2 adsorption versus coverage are shown in Fig. 3 and the amounts of adsorbed CO_2 are reported in Table 1. As can be seen, the initial heats of adsorption (near zero coverage) are relatively low as compared to bulk MgO (∼120 kJ/mol), around 70 kJ/mol for the three samples. However, the adsorbed amount of CO_2 and the distribution of the strength of adsorption, i.e., basicity, are strongly dependent on MgO content. Thus, for low to medium MgO contents (after 5 and 10 wt.% MgO addition), the total amount of adsorbed CO_2 is equal to 0.013 and 0.037 µmol/m^2, respectively, and the basicity strength declines rapidly upon CO_2 adsorption. In contrast, the Co/35 wt.% MgO–SiO_2 catalyst presents a rather large amount of medium strength basic sites with a total amount of adsorbed CO_2 of about 0.164 µmol/m^2 (Table 1). With respect to the previous XRD and TPR conclusions, the weak basicity for low to medium MgO content can be related to the formation of the solid solution Co–Mg–O while the larger and stronger basicity for high MgO content can be ascribed to the absence of such a solid solution (due to the silicate overlayer formation) and therefore the presence of accessible basic MgO sites for CO_2 adsorption.

3.4. Catalytic performances

The effect of MgO addition on catalytic performance of the reference Co/SiO_2 catalyst is presented in Table 1, Figs. 4 and 5.

3.4.1. Temperature cycles

Fig. 4A and B report the changes in CO_2 and CH_4 conversion upon temperature increase from 500 to 800 °C and decrease back to 500 °C. The dashed lines correspond to the calculated thermodynamic equilibria, based on the gaseous reactants—CH_4, CO_2 and products—H_2, CO, H_2O species (Gibbs free energy minimization method).

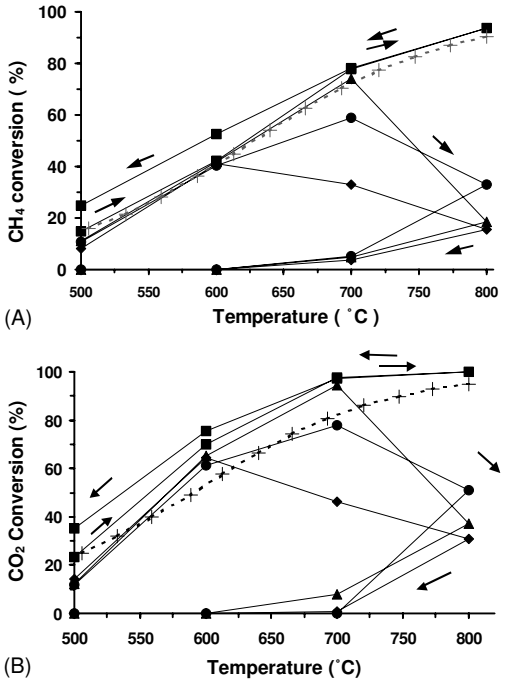

Fig. 4. Influence of reaction temperature on CH_4 (A) and CO_2 (B) conversion over (■) Co/35 wt.% MgO–SiO_2, (●) Co/10 wt.% MgO–SiO_2, (▲) Co/5 wt.% MgO–SiO_2 and (◆) Co/SiO_2 catalysts. Calculated equilibrium conversions (+). Reaction conditions: P_{tot} = 1 atm, CH_4/CO_2/He = 10/10/80 vol.%, cobalt loading = 5 wt.%.

As can be seen, by increasing the temperature from 500 to 600 °C, methane and carbon dioxide conversion follow approximately the values corresponding to the thermodynamic equilibrium for all catalysts, which is expected for the rather low space velocity used for this catalytic test (SV = 12, 000–13, 000 $cm^3/h\,g_{cat}$). Then the conversion starts to decrease after 600 °C for the unpromoted Co/SiO_2, after 700 °C for the 5 and 10 wt.% MgO containing samples, the residual conversion at 800 °C being close to the initial one at 500 °C. By decreasing the temperature, the conversion rapidly vanishes for these three samples.

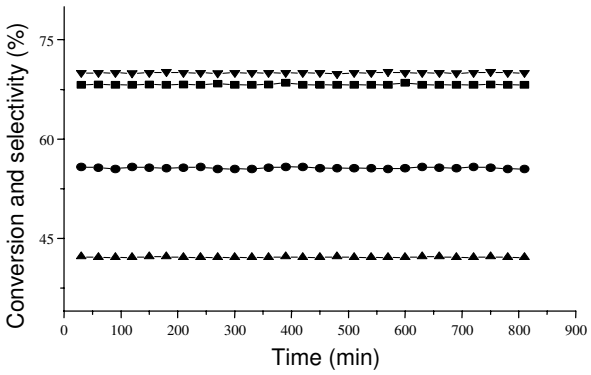

Fig. 5. Stability test for the Co/35 wt.% MgO–SiO_2 sample: (▼) CO_2 conversion, (▲) CH_4 conversion, (■) H_2 selectivity and (●) CO selectivity. Reaction temperature = 600 °C, P_{tot} = 1 atm, CH_4/CO_2/He = 10/10/80 vol.%.

Unless these 3 catalysts, the Co/35 wt.% MgO–SiO_2 sample permanently tends to equilibrate the effluent composition over the whole temperature range. It can even be noted, taking into account the uncertainties of the kinetic measurements, that methane but essentially carbon dioxide conversions slightly exceed the calculated equilibrium values, especially when decreasing temperature after the high temperature cycle.

This trend for CO_2 conversion to overpass the predicted equilibrium values, also outlined in Table 1 for initial conversion at 600 °C, can have several origins: (i) a trapping effect of CO_2 by the basic sites of the surface may contribute to displace the equilibrium towards higher conversions. However, such an effect would only be transient till the adsorption capacity of the surface is reached; (ii) most likely, side reactions like the Boudouard equilibrium $C + CO_2 \rightarrow 2CO$ or the methane cracking $CH_4 \rightarrow C + 2H_2$ also contribute to the reactants consumption without being strictly accounted for in equilibrium calculation. As a matter of fact, the exact nature of the carbon formed under reaction conditions (graphite, filaments, amorphous, etc.) is known only in a qualitative way and therefore the equilibrium values remain quite approximate.

As for the improved conversion which is observed for the highly MgO loaded sample after high temperature tests (Fig. 4A and B), it indicates that the concentration of active site is increased during this period, presumably due to an additional cobalt phase reduction occurring during high temperature reaction steps.

3.4.2. Steady-state testing conditions

The catalytic stability of all the samples was also tested under steady-state isothermal conditions at 600 °C for 3 h (after in situ reduction in pure hydrogen at the same temperature) as reported in Table 1. It is observed that the three MgO free or weakly doped samples which were initially active enough to reach the equilibrium (or overpass it, as discussed before) severely deactivate during this short period, at variance with the Co/35 wt.% MgO–SiO_2 catalyst which displays neither activity nor selectivity changes under these conditions. For the latter, long term lab-scale stability tests performed during 30 h confirmed the unique behaviour of this sample as compared to the other ones (Fig. 5).

3.4.3. Coke deposition

From Table 1, it clearly comes that the coke formation (measured by temperature programmed oxidation carried out after catalyst testing) is important for the unpromoted and low to medium MgO-doped samples (from 0.3 to 0.4 wt.% after 12 h on stream at 600 °C) while only traces of carbon were detected on the highly MgO-doped sample. This trend to be coke resistant for the most stable catalyst was also confirmed by additional experiments carried out under conditions more favorable for coke deposition (CH_4/CO_2 ratio = 2/1 instead of 1/1 like in the present investigation) (unpublished results). For that case, TEM study revealed that,

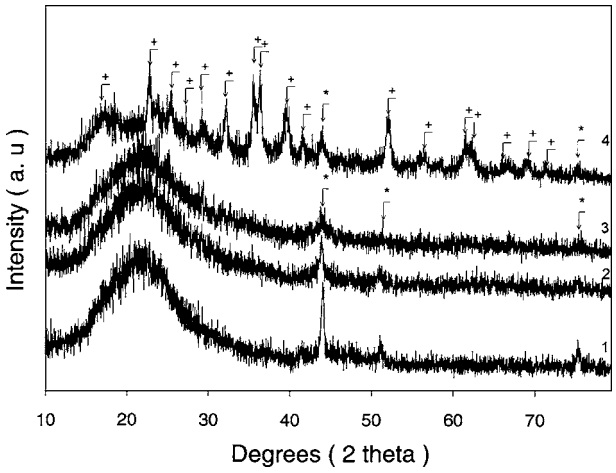

Fig. 6. XRD patterns of (1) Co/SiO_2, (2) Co/5 wt.% $MgO–SiO_2$, (3) Co/10 wt.% $MgO–SiO_2$ and (4) Co/35 wt.% $MgO–SiO_2$ used catalysts: (*) Co, (+) Mg_2SiO_4. After cycle of sequential changes in reaction temperature.

while only very small graphite-like species could be observed with the highly MgO-doped sample, most of the coke deposition for the deactivating samples was under the form of filaments and bi-dimensional graphite encapsulating the cobalt particles.

3.4.4. Structure changes upon testing

The XRD analysis of the catalysts after temperature testing cycles is presented in Fig. 6. For the unpromoted sample and the low to medium MgO content samples (5–10 wt.% MgO addition), a strong effect of the dry reforming reaction is observed which transformed the bands characteristic of the Co_3O_4 phase observed after calcination (Fig. 1) into bands characteristic of metallic cobalt of FCC structure. By applying to the latter the Scherrer formula allowing us to evaluate the average particle size [30], it comes that the poor dispersion of the cobalt phase for the MgO free sample (about 7%, corresponding to an average particle size of 17 nm) tends to increase after MgO addition (till up to about 20%, corresponding to an average particle size of 5 nm). This feature obviously corresponds to the strong interaction Co–Mg–O as previously postulated, tending to stabilise the cobalt phase during its reduction under reforming conditions. However, this interaction does not prevent the active phase to be severely deactivated after high temperature testing.

For the case of the highly MgO loaded sample, Co/35 wt.% $MgO–SiO_2$, it is observed that the magnesium silicate phase, initially detected as a minor phase after calcination, is reinforced and forms now the main crystallised phase supporting a well dispersed metallic cobalt phase (20–25%). These results indicate that for this high content of MgO, the formation of the Mg_2SiO_4 phase under reaction conditions not only promotes the formation of well dispersed cobalt particles but also prevents their sintering at high temperature.

3.4.5. In situ DRIFT measurements

In order to understand the origin of catalysts aging in line with the dry reforming mechanism, in situ DRIFT experiments were carried out under CH_4/Ar and CO_2/Ar flows and under reacting conditions, i.e, under $CH_4/CO_2/Ar$ flow at 600 °C.

For the three deactivating catalysts $Co(O)/SiO_2$, Co(O)/5% $MgO–SiO_2$ and Co(O)/10% $MgO–SiO_2$, no resolved enough IR spectra could be recorded, due to a very fast carbon deposition occurring under reaction conditions.

In contrast, reasonably well resolved in situ DRIFT spectra could be recorded on Co/35% $MgO–SiO_2$ catalyst (Fig. 7A and B). The main bands (not reported here) are related, as expected, to the gas phase absorption with (i) the C–H vibration of gaseous methane at 3014 cm^{-1} and its harmonic band at 1330 cm^{-1} under methane atmosphere, (ii) the large CO_2 gaseous rotation–vibration P and R bands at 2360 and 2340 cm^{-1}, respectively, under CO_2 atmosphere and (iii) the two band sets of gaseous methane and carbon dioxide observed under dry reforming reaction conditions. For the latter, the slight doublet at 2200–2000 cm^{-1} characteristic of the gaseous CO was also observed, attesting that the dry reforming reaction does proceed in the DRIFT cell but at a lower conversion than in the tubular reactor used

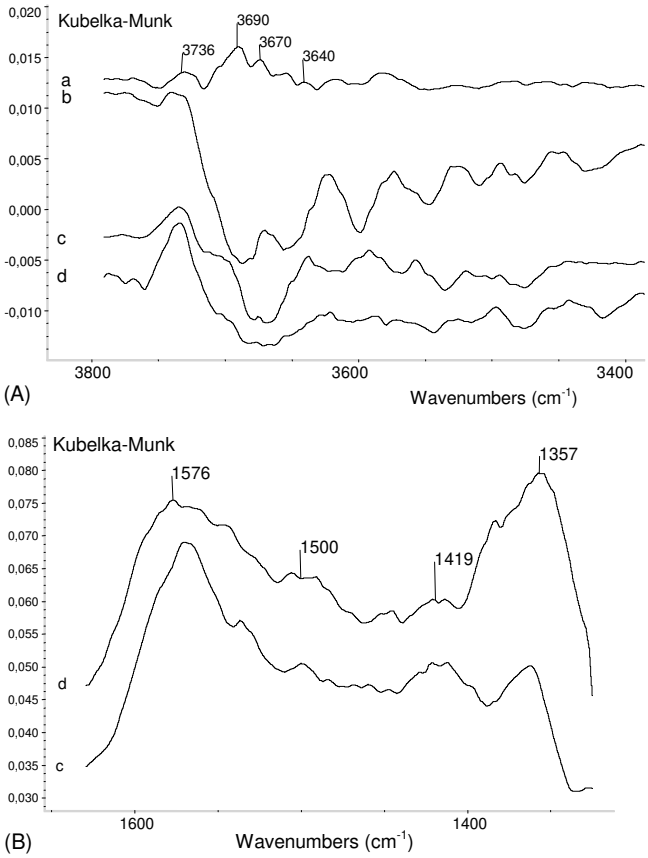

Fig. 7. DRIFT spectra of Co/35 wt.% $MgO–SiO_2$, recorded at 600 °C: (a) under flowing He; (b) under flowing $CH_4/He = 10/90$ vol.%; (c) under flowing $CO_2/He = 10/90$ vol.% and (d) under flowing reacting mixture $CH_4/CO_2/He = 10/10/80$ vol.%.

for the kinetic studies for similar conditions. As a matter of fact, large temperature gradients arising from the cell geometry (the KBr windows located at few millimeters from the 600 °C bed have to be maintained at room temperature) prevent from any strict temperature control in the DRIFT catalytic bed.

In addition to the large gas phase bands above mentioned, other smaller bands due to adsorbed species are detected in the range 3800–3400 and 1600–1300 cm^{-1}, respectively. On the reference spectrum recorded after reduction under hydrogen at 600 °C (Fig. 7A(a)), only OH bands are observed at 3736 (weak), 3690 (main), 3670 (shoulder) and some residual bands at lower frequencies. The highest frequency band remains almost unchanged under CH_4 (Fig. 7A(b)), tends to increase under CO_2 (Fig. 7A(c)) and even more under CH_4/CO_2 reacting mixture (Fig. 7A(d)). This indicates without ambiguity its inert character towards the reforming gases. It corresponds to the usual silanol Si–OH groups and therefore can be assigned to the silicate layer, which crystallinity is reinforced under reacting conditions, as demonstrated by XRD measurements. In contrast the bands at 3690 and 3670 cm^{-1} tend to disappear under CH_4, CO_2 and CH_4/CO_2 atmospheres since a negative signal is observed after subtracting the reference spectrum (Fig. 7A(b–d)). This indicates their strong reactivity towards the related reforming gases, but at relatively distinct rates. Thus, under methane flow, the band at 3690 cm^{-1} is essentially affected, while the band at 3670 cm^{-1} is still observed (Fig. 7A(b)). Note that the high noise level can be ascribed to the carbon deposition occurring from methane cracking in the absence of oxidizing gas. In contrast, the band at 3670 cm^{-1} tends to strongly be consumed under CO_2 flow (Fig. 7A(c)) but at a lesser extent under CH_4/CO_2 reacting mixture (Fig. 7A(d)). From these observations, it comes that the band at 3690 cm^{-1} could correspond to cobalt hydroxide species Co(OH) still present even after reduction due to the remaining traces of humidity always present in the dynamic DRIFT cell, as attested by the background water signal recorded downstream by mass spectrometry. These species would react with methane according to:

$$2Co(OH) + CH_4 \rightarrow Co_2C + 2H_2O + H_2 \quad (2)$$

On the other hand, in the 1600–1200 cm^{-1} range, where very small preexisting bands was observed on the reference spectrum (not shown here), new large bands are formed under CO_2 atmosphere (Fig. 7B(c)), therefore corresponding to basic sites able to react with the acidic carbon dioxide, as attested by the calorimetric measurements above reported. According to numerous references [25], these bands can be attributed (i) to carbonates formed on the basic sites of the magnesia additive, most likely as a complex combination of mono- and bi-dentate species [25,26], and/or (ii) to hydrogeno-carbonate or bicarbonate species HCO_3^- formed on Mg–OH groups of the Mg_2SiO_2 silicate layer. It can be noted that under CO_2 atmosphere, no CO vibration was detected in the range 2200–1800 cm^{-1}, which means that CO_2 activation, when occurring on Co/35% MgO–SiO_2 in addition to the carbonatation above mentioned, does not lead to accumulation of metal-adsorbed CO according to:

$$CO_2 = CO_{ads} + O_{ads} \quad (3)$$

From this formation of carbonate and hydrogeno-carbonate, even reinforced under the dry reaction conditions (spectrum 7Bd), one may assume as previously suggested the direct reaction of gaseous carbon dioxide with the basic surface hydroxyl groups according to:

$$CO_2 + OH^- \Leftrightarrow HCO_3^- \quad (4)$$

Simultaneously, methane dissociates on cobalt particles into gaseous hydrogen and surface carbon, as generally assumed for methane cracking on non noble metals Ni or Co [27]:

$$CH_4 + Co \rightarrow Co\text{–}C + 2H_2 \quad (5)$$

The immediate vicinity of the hydrogeno-carbonate species accumulated around the cobalt particles via the silicate layer would then allow their decomposition into carbon monoxide and active oxygen able to oxidize the surface carbon into CO and restored active sites. The lumped elementary steps corresponding to that process can tentatively be written as:

$$HCO_3^- + Co\text{–}C \rightarrow 2CO + OH^- + Co \quad (6)$$

As such, the specificity of the above described mechanism is that the surface carbon Co–C cannot be transformed into bulk carbide, Co_2C, precursor of filament or encapsulating carbon, due to the permanent reservoir of active oxygen [27]. This, in addition to the structural stability of the small cobalt particles strongly interacting with the silicate overlayer, explains now quite well the catalytic stability of the related system, as measured under the present operating conditions. Similar effects involving the presence of surface carbon–oxygen containing species (like carbonates) around the metal particles were also reported on some other highly stable systems such as La_2O_3/Ni [28] or MgO–Ru/activated carbon [29]. For the present case, the excellent thermal stability of the silicate layer brings an additional advantage as compared to the quoted systems.

Note, as suggested previously, that the reaction steps (2) (4) and (5) which correspond to surface accumulation of reactants would contribute to the observed displacement of thermodynamic equilibrium.

4. Conclusion

By adding magnesia to a Co/silica catalyst, it was demonstrated that very positive effects on catalyst stability arise from the formation of a magnesium silicate phase for a tuned amount of MgO additive. First, this phase prevents cobalt phase sintering by avoiding particle coalescence, which is the main sintering process under these reacting conditions.

Second, the specific medium basicity of the silicate adlayer, revealed by calorimetric measurements, allows a reversible storage of a pool of hydrogeno-carbonates in the vicinity of Co particles, ensuring a constant feed in surface oxygen and therefore the immediate oxidation of surface carbide formed from methane cracking into carbon monoxide. As such, this bi-functional process hinders deactivating carbon formation: (i) by limiting bulk cobalt carbide and therefore carbon filament formation, which may lead to reactor plugging and/or particle fragmentation, and (ii) by suppressing encapsulating carbon formation which limits access of reactant to the active cobalt phase.

Acknowledgements

The "Comité Mixte d'évaluation et prospective de la coopération interuniversitaire franco-algerienne (CMEP)", the French Embassy at Algiers are gratefully acknowledged for financial support. Dr. G. Bergeret and M.T. Gimenez from the XRD scientific service at IRC are also fully acknowledged for fruitful experiments and discussion.

References

[1] M.C.J. Bradford, M.A. Vannice, Cat. Rev. - Sci. Eng. 41 (1999) 1.
[2] J.H. Edwards, Catal. Today 23 (1995) 29.
[3] V.C.H. Kroll, H.M. Swaan, C. Mirodatos, J. Catal. 161 (1996) 409.
[4] H.M. Swaan, V.C.H. Kroll, G.A. Martin, C. Mirodatos, Catal. Today 21 (1994) 571.
[5] D. Halliche, R. Bouarab, O. Cherifi, M.M. Bettahar, Stud. Surf. Sci. Catal. 119 (1998) 705.
[6] Q. Zhuang, Y. Qin, L. Chang, Appl. Catal. 70 (1991) 1.
[7] A. Guerrero-Ruiz, A. Sepulveda-Escribano, I. Rodriguez-Ramos, Catal. Today 21 (1994) 545.
[8] J.S. Choi, K.I. Moon, Y.G. Kim, J.S. Lee, C.H. Kim, D.L. Trimm, Catal. Lett. 52 (1998) 43.
[9] D. Halliche, R. Bouarab, O. Cherifi, M.M. Bettahar, Catal. Today 29 (1996) 373.
[10] J. Nakamura, K. Aikawa, K. Sato, T. Uchijima, Catal. Lett. 25 (1994) 265.
[11] K.B. Mok, J.R.H. Ross, R.M. Sambrook, in: G. Poncelet et al. (Eds.), Preparation of Catalysts, vol. III, Elsevier, Amsterdam, 1983, p. 291.
[12] L.B. Backman, A. Rantiainen, A.O.I. Krause, M. Lindblad, Catal. Today 43 (1998) 11.
[13] E. van Steen, G.S. Swell, R.A. Makhathe, G. Micklethwaite, H. Manstein, M. de Lange, C.T. O'Connor, J. Catal. 162 (1996) 220.
[14] R.C. Reuel, C.H. Bartholemew, J. Catal. 85 (1984) 63.
[15] H. Ming, B.G. Baker, Appl. Catal. 123 (1995) 23.
[16] R. Srinivasan, R.J. De Angelis, P.J. Reucroft, A.G. Dhere, J. Bentley, J. Catal. 116 (1989) 144.
[17] E. Ruckenstein, H.Y. Wang, Appl. Catal. 204 (2000) 257.
[18] G. Choi, Catal. Lett. 35 (1995) 291.
[19] G.J. Haddad, J.G. Goodwin Jr, J. Catal. 157 (1995) 25.
[20] R. Bouarab, O. Cherifi, J. Alger. Chem. Soc. 9 (1999) 99.
[21] JCPDS Powder Diffraction File no. 42-1467.
[22] F. Liebau, Structural Chemistry of Silicates, Springer-Verlag, Berlin, 1985.
[23] JCPDS Powder Diffraction File no. 34-0189.
[24] A. Lapidus, A. Krylova, V. Kazanskii, V. Borokov, A. Zaitsev, J. Rathousky, A. Zukal, M. Jancalkova, Appl. Catal. 73 (1991) 65.
[25] G. Socrates, Wiley, Chichester, 1994.
[26] V.A. Kiselev, V.O. Krylov, Adsorption and Catalysis on Transition Metals and their Oxides, Springer-Verlag, Berlin, 1989.
[27] L. Pinaeva, Y. Schuurman, C. Mirodatos, in: M. Maroto-Valer, C. Song, Y. Soong (Eds.), Environmental Challenges and Greenhouse Gas Control for Fossil Fuel Utilization in the 21st Century, Plenum Press, New York, 2002, p. 313.
[28] A. Slagtern, Y. Schuurman, C. Leclercq, X. Verykios, C. Mirodatos, J. Catal. 172 (1997) 118.
[29] P. Ferreira-Aparicio, C. Márquez-Alvarez, I. Rodríguez-Ramos, Y. Schuurman, A. Guerrero-Ruiz, C. Mirodatos, J. Catal. 184 (1999) 202.
[30] G. Bergeret, P. Gallezot, in: G. Ertl, H. Knözinger, J. Weitkamp (Eds.), Handbook of Heterogeneous Catalysis, vol. 2, Wiley-VCH, Weinheim, 1997, p. 447.